JOURNAL OF GEOPHYSICAL RESEARCH, VOL. 102, NO. D15, PAGES 18,981-18,995, AUGUST 20, 1997

Composition of the troposphere over the Indian Ocean during the monsoonal transition

Kevin P. Rhoads,[1] Paul Kelley,[2] Russell R. Dickerson,[2] Thomas P. Carsey,[3] Michael Farmer,[3] Dennis L. Savoie,[4] and Joseph M. Prospero[4]

Abstract. The atmosphere over the equatorial Indian Ocean is a unique environment in which to study the chemical and radiative effects of an intense source of anthropogenic emissions from the northern hemisphere directly coupled to the relatively pristine background conditions present in the southern hemisphere. As an initial investigation into the role of the intertropical convergence zone (ITCZ) on interhemispheric transport of pollutants, a number of trace atmospheric species were measured aboard the National Oceanic and Atmospheric Administration (NOAA) R/V *Malcolm Baldrige* between Durban, South Africa, and Colombo, Sri Lanka, from March 12 to April 22, 1995. Sharp increases in the concentrations of carbon monoxide (CO), carbon dioxide (CO_2), and aerosols were associated with four distinct meteorological regimes transected by the cruise track from 33°S to 9°N. Across the ITCZ, aerosol concentrations, including non-sea-salt sulfate, nitrate and ammonium, increased by a factor of 4. Surface ozone measurements showed a latitudinal gradient with a minimum near the equator and a strong diurnal variation in the equatorial regions. The latitudinal profile of gas-phase reactive nitrogen paralleled ozone and was higher in the remote southern hemisphere than in the remote northern hemisphere. Evidence of direct anthropogenic impact on the region was observed more than 1500 km from the southern tip of India. Back trajectories, calculated with NOAA's medium range forecast data using the Hybrid Single-Particle Lagrangian Integrated Trajectory (HY-SPLIT) program, identified the origin of the air mass regimes characterized by the trace gas and aerosol data. Continental emissions in the northern hemisphere were shown to have a major impact on the radiative properties and oxidizing capacity of the marine atmosphere.

Introduction

It is often difficult to discern the role of anthropogenic emissions on the chemistry of the remote atmosphere because of our inability to define adequately natural background conditions. The Indian Ocean, bordered to the south by one of the most sparsely populated areas on Earth and to the north by the densely populated and rapidly developing Indian subcontinent, is a unique environment in which to study the large-scale impact of air pollutants on marine tropospheric chemistry and cloud properties. The large-scale atmospheric circulation in this region is dominated by a complete biannual reversal in the low-level winds associated with the Indian monsoon. This flow pattern is largely driven by the heat gradient between the Indian subcontinent and the ocean as a result of the seasonal change in solar zenith angle [*Cadet*, 1979]. In the winter months the atmosphere over the continental areas in the north cools relative to the ocean, forming a region of general subsidence. This high-pressure system gives rise to the Indian dry season and generates a persistent northeasterly offshore flow. Under the intense insolation of the summer months, heat lows develop over the land mass areas in the north, reversing the circulation and producing a moisture rich southwesterly onshore flow that brings torrential rains over India. During the transition period between the northeast monsoon (December-February) and the southwest monsoon (June-August), zonal temperature gradients and easterlies in the Indian Ocean tropics are weak with the intertropical convergence zone (ITCZ) typically found at about 10°S. At this time the cross-equatorial monsoonal flow may provide a mechanism by which the northern hemisphere air, laden with continental aerosols, anthropogenic sulfates, and reactive gases, is coupled to the relatively pristine air of the southern hemisphere at the conflux of the two air masses into the ITCZ.

There are very few measurements of trace chemical species from the Indian Ocean. The 1987 Soviet American Gases and Aerosols (SAGA) cruise traversed the eastern portion of the Indian Ocean at the end of June along 90°E from 30°S to about 5°N [*Johnson et al.*, 1990]. The surface data collected showed a strong latitudinal gradient in ozone concentration from about 30 parts per billion by volume (ppbv) at 30°S to 10 ppbv at 10°S and then remained relatively constant through the ITCZ to 5°N. Similar gradients were observed in the Pacific Ocean with a minimum of less than 5 ppbv found near the ITCZ. Ozone profiles from a year of soundings made at Reunion Island (56.6°E, 22.1°S) [*Baldy et al.*, 1996] showed a strong seasonal variation in total tropospheric ozone that approximately follows the seasonal biomass burning activities in southeastern Africa and Madagascar. During the burning season from September to November (austral spring), layers of

---

[1] Department of Chemistry, University of Maryland, College Park.

[2] Department of Meteorology and the Center for Clouds, Chemistry and Climate, University of Maryland, College Park.

[3] Atlantic Oceanographic and Meteorological Laboratory, NOAA, Miami, Florida.

[4] Rosenstiel School of Marine and Atmospheric Science, University of Miami, Florida.

Paper number 97JD01078.
0148-0227/97/97JD-01078$09.00

high ozone were observed in strata influenced by westerlies above the inversion level that could be traced back to the African continent. From January to March, biomass burning is greatly reduced. The sounding data from this period suggest that convective cells near the ITCZ enhance the autumn tropospheric ozone minimum by lofting marine boundary layer air containing little ozone and high relative humidity.

Strong seasonal and latitudinal variations have also been observed in the aerosol and precipitation composition in the region. *Chester et al.* [1991] reported mineral dust concentrations decreasing from 15-20 $\mu g\ m^{-3}$ in the north to 0.01-0.25 $\mu g\ m^{-3}$ below 35°S in the far southern ocean. The authors noted that the seasonal reversal of the predominate wind flow that accompanies the monsoonal inversion in the northern ocean does not affect southeasterly winds in the southern ocean region (south of about 10°S). *Savoie et al.* (1987) have shown that there are also strong gradients in the concentrations of particulate nitrate and sulfate with the highest values for both species found in the north. Precipitation samples collected from Amsterdam Island (77.5°E, 37.7°S) [*Galloway and Gaudry,* 1984; *Moody et al.,* 1991] indicate that the central southern Indian Ocean is generally representative of pristine marine conditions comparable to that of the remote Pacific [*Prospero and Savoie,* 1989]. Occasionally, air masses showing evidence of strong anthropogenic impact were identified which significantly contributed to both the average concentrations and total deposition observed [Moody et al., 1991]. These episodes were characterized by particularly high nitrate (NO_3^-) and non-sea-salt sulfate (SO_4^{2-}) levels from Africa and Australia.

Gradients in aerosol optical thickness (AOT) determined from advanced very high resolution radiometer (AVHRR) measurements suggest that there are two dominant sources for aerosols over the Arabian Sea. High values of AOT are seen over the northern end of the Arabian Sea. This is believed to be due to soil dust derived from sources in the Arabian Peninsula and from soils in the Tigris and Euphrates basin [*Ackerman and Cox,* 1989; *Prospero,* 1981], although soils in the arid regions of NW India and East Africa could also contribute [*Ackerman and Cox,* 1989]. The seasonality of dust storms and haze conditions in this region [*Ackerman and Cox,* 1989] is consistent with the seasonality of the AOT distributions observed in AVHRR [*Husar et al.,* 1997]. The dust concentrations over the Arabian Sea are comparable to those measured in the Mediterranean and off the west coast of Africa [*Savoie et al.,* 1987; *Prodi et al.,* 1983], and the seasonality is consistent with the dust transport distributions shown in AVHRR and with the monsoon circulation [*Ackerman and Cox,* 1989]. Dust concentrations drop sharply as one moves from the Arabian Sea southward into the southern hemisphere circulation [*Savoie et al.,* 1987; *Prodi et al.,* 1983]. A second major source of Arabian Sea aerosols is located in southern India as suggested by a prominent bulge in the AOT distributions along the SW coast of India from about 15°N to the southern tip. This aerosol plume appears to be attributable to pollution sources not soil dust. Dust storm statistics suggest that there are major sources of mineral dust in northern India [*Ackerman and Cox,* 1989] but that there is very little dust storm activity in southern India below 15°N at any time of year. AVHRR suggests that during the spring there are very few major sources of aerosols evident in the Indian Ocean south of the equator. Biomass burning is not active at this time of year. In Oceanea, burning appears to peak in September-October [*Malingreau et al.,* 1985], the end of the dry season. In southern Africa, burning occurs mostly in July-September [*Andreae et al.,* 1994], consistent with the prominent plumes observed in AVHRR [*Husar et al.,* 1997].

As an exploratory experiment to investigate interhemispheric differences in Indian Ocean tropospheric chemistry, instruments were installed aboard the National Oceanic and Atmospheric Administration (NOAA) R/V *Malcolm Baldrige* during the World Ocean Circulation Experiment (WOCE) I5/I7 repeat leg from South Africa to Sri Lanka. This paper will concentrate on the meteorological observations during the cruise, the surface CO, NO, NO_2, NO_y and O_3 measurements, as well as bulk aerosol data. In addition, the results of NO_2 photolysis rate coefficient and aerosol optical depth determinations will be presented. The results from 20 ozonesondes and a discussion of the diurnal variation in boundary layer ozone will be presented separately.

Experimental Techniques

The NOAA R/V *Malcolm Baldrige* departed Durban, South Africa (29.8°S, 26.1°E) on March 21, 1995 (Julian day (J.D.) 80) and arrived in Colombo, Sri Lanka (6.7°N, 79.6°E), on April 22 (J.D. 112) travelling on the cruise track shown in Figure 1. The ship's primary mission was to conduct oceanographic research which required the ship to remain stationary for considerable time each day (up to 15 hours). These stationary periods interrupted sampling when ship diesel exhaust was carried past the intakes, as discussed below.

Aerosol Sampling and Aerosol Optical Depth

Bulk aerosol samples were collected for major ion analysis on top of a 10 m tower mounted 5 m aft of the ship's bow. Total height above the sea surface was ~15 m. Aerosol particles were collected by drawing ambient air through a 20 x 25 cm Whatman-41 filter at a flow rate of about 1 $m^3\ min^{-1}$. These filters have total mass collection efficiencies of greater than 90% for non-sea salt (NSS) sulfate (SO_4^{2-}), 95% for nitrate (NO_3^-) and sea salt, and 99% for mineral dust [*Savoie et al.,* 1989a]. Because Whatman-41 and other cellulose filters that are coated with NaCl are known to collect HNO_3 vapor with high efficiency, we consider our measured NO_3^- concentrations to be those of total inorganic NO_3^-, i.e., particulate NO_3^- plus gaseous HNO_3 [*Savoie et al.,* 1989b]. However, the concentration of gaseous HNO_3 in the near-surface marine boundary layer is typically around 20% or less of the total NO_3^- [*Savoie and Prospero,* 1982]. The concentration of ammonium (NH_4^+) reported here should be regarded as the total of aerosol NH_4^+ plus any gas-phase ammonia (NH_3) that might react with acid aerosol species on the filter (e.g., NSS SO_4^{2-} and NO_3^-).

To avoid contamination from the ship itself, a weather vane and an anemometer on top of the 10 m bow tower were connected to circuitry that limited sampling to flow for at least 10 s at a minimum speed of 2 $m\ s^{-1}$ from a 270° sector centered on bow. Filters were changed twice a day and transferred to a freezer for storage. A blank sample was created for every four exposed filters by manipulating an unexposed filter through the sampling protocol without actually drawing air through it. Upon arrival at Colombo, Sri Lanka, the samples were packed in dry ice and shipped to the Rosenstiel School of Marine and Atmospheric Sciences, Miami, Florida. After extracting the filter papers with ultapure water, the extracts were analyzed for

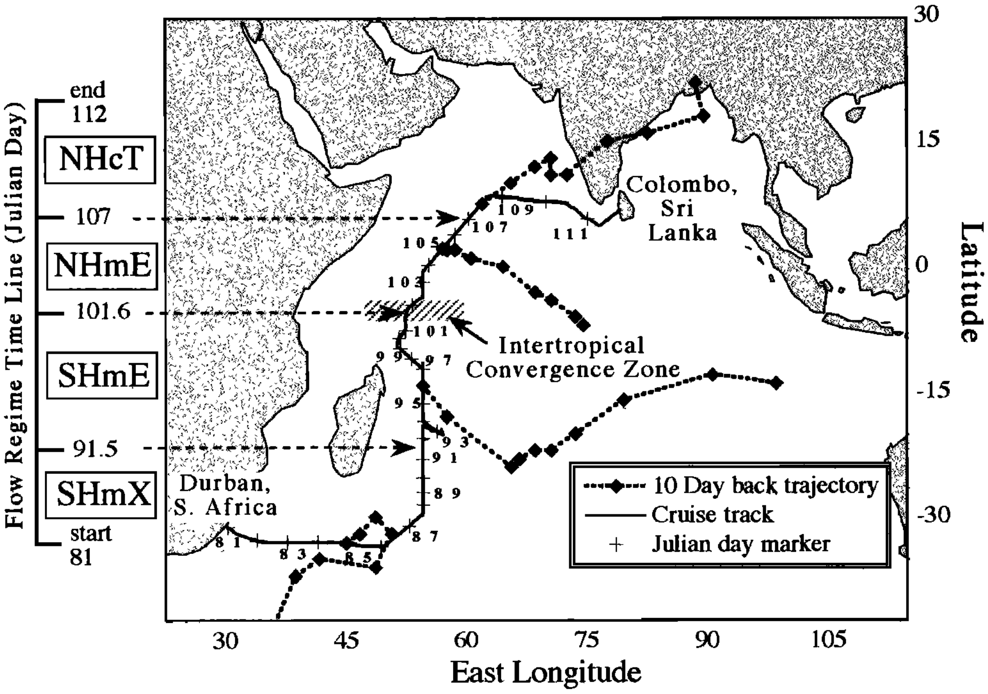

Figure 1. The cruise track (solid line) and representative 10 day back trajectories (dashed lines) for the four flow regimes encountered calculated from the National Oceanic and Atmospheric Administration's (NOAA) Medium Range Forecast (MRF) database using the Hybrid Single-Particle Langrangian Integrated Trajectories (HYSPLIT) model. The trajectories have diamonds indicating a 1 day time step and have endpoint altitudes of 1 km. The four flow regimes are coded as SHmX, southern hemisphere marine extratropical; SHmE, southern hemisphere marine equatorial; NHmT, northern hemisphere marine equatorial; and NHcT, northern hemisphere continental tropical.

sodium (Na^+) within ±2% by flame atomic absorption, NH_4^+ within ±5% by automated colorimetry, and chloride (Cl^-), NO_3^-, and SO_4^{2-} within ±5% by ion chromatography. Non-sea salt sulfate was calculated as total SO_4^{2-} minus Na^+ multiplied by 0.2517, the mass ratio of SO_4^{2-} : Na^+ [*Savoie et al.*, 1992]. The mineral dust collected was quantified within ±10% by ashing the extracted filter paper at 500°C and weighing the residue.

Aerosol optical thickness measurements were made using an EKO sunphotometer (Model MS-120, EKO Instruments, Tokyo, Japan) operating at peak wavelengths of 500, 675, 875, 945 nm. This instrument was calibrated 3 months before the voyage at the World Radiation Center (Davos, Switzerland), and the linearity was reported to be 0.3%. The estimated wavelength accuracy of the dielectric thin film interference filters is ±2 nm with a half bandwidth of 5-6 nm [*Pinker et al.*, 1994]. Because of the movement of the ship the instrument was aligned by hand, and the measurements were recorded as the maximum signal obtained using the peak-picking function of the device. Only a few useful observations were collected during the voyage because of excessive ship roll and cloudiness.

CO and CO_2 Measurements

Sample air for continuous carbon monoxide (CO) measurements was drawn through a 0.5 μm Teflon inlet filter mounted at the 7 m level on the bow tower. A modified commercial nondispersive infrared gas filter correlation CO analyzer (Model 48, Thermo Environmental Instruments, Franklin, Massachusetts) located 30 m away was used with a flow rate of 1.0 L min^{-1}. Chemical zeroing of the instrument was performed at 20 min intervals by switching the sample flow through a Pd/Al_2O_3 catalyst (Degussa Corp., Plainfield, New Jersey, type E 221 P/D) heated to 250°C [*Dickerson and Delany*, 1988; *Doddridge et al.*, 1994]. Weekly calibrations were performed using a secondary standard of 0.97 parts per million by volume (ppmv) (Scott-Marrin, Inc., Riverside, California) previously referenced to a National Institute of Standards and Technology (NIST) standard. A small change in calibration (~4%) over the period of the cruise was attributed to degradation of the Pd/Al_2O_3 catalyst. A background time series was created by linearly interpolating between zero modes. After subtracting the background data the 30 s values were used to calculate hourly averages that show an uncertainty of about ±5 ppbv (±1σ).

Measurements of atmospheric CO_2 concentrations were made using a nondispersive infrared CO_2 analyzer (Model LI-6251, Li-COR, Lincoln, Nebraska). This instrument compares the absorption due to ambient CO_2 to that due to a CO_2 reference gas. The analyzer operated in a differential mode, with a "zero" reference gas of CO_2 at about 10 ppmv below ambient levels flowing continuously through the reference cell of the instrument. Ambient air was drawn from the bow of the ship through Decoron tubing at about 5 L min^{-1}. Before entering the analyzer the sample stream passed through a water vapor trap, a particle filter, and a flowmeter. The instrument was calibrated at 1 hour intervals using three CO_2 reference gases. This technique has an absolute accuracy of ±0.5 ppmv with the precision estimated at ±0.15 ppmv CO_2 [*Wanninkhof and Thoning*, 1993].

Ozone Measurements

Continuous ozone measurements were made using a commercial UV absorption instrument (Model 300, Environics, Inc., West Willington, Connecticut) as described by *Piotrowicz et al.* [1990]. Sample air was drawn through Teflon tubing with an in-line 0.5 µm Teflon filter mounted on the top deck of the ship approximately 14 m above the surface. Intake line losses of ozone were determined to be less than 5%. Daily checks of instrument background were made by passing the sample flow through a small volume of Hopcalite catalyst (Mine Safety Appliances Co., Pittsburgh, Pennsylvania). Zero mode detection limit was 0.45 ppbv (S:N=1:1, ±2σ) using 30 s averaging. Over the course of the cruise, zero mode measurements varied by less than 2 ppbv and showed no diurnal variation.

NO, NO_2, and NO_y Measurements

Nitric oxide (NO) measurements were made with an ozone chemiluminescence instrument built by NOAA's Atlantic Ocean Marine Laboratory (AOML) [*Carsey et al.*, 1997] on the basis of the design developed by *Ridley et al.* [1988]. This instrument used a photon counter to collect emission events over 10 s intervals and showed a sensitivity to NO of approximately 4 counts/parts per trillion by volume (pptv) with a zero mode detection limit of about 18 pptv (10 s, S:N=1:1, ±2σ). The detector sampled 1.0 L min^{-1} at the 7 m level of the bow tower from one of two inlets: a combined NO/NO_2 inlet or a NO_y inlet leading directly to a tower-mounted Mo converter maintained at 380°C [*Luke and Dickerson*, 1987; *Fehsenfeld et al.*, 1987; *Nunnermacker*, 1990]. Ambient air was drawn through these inlets with in-line Teflon filter holders housing 0.5 µm Teflon filters that were changed at least once each day. The concentration of NO_2 was determined by reduction to NO using a broadband UV photolytic converter [*Kley and McFarland*, 1980; *Carroll et al.*, 1992, *Poulida et al.*, 1994]. The instrument was typically cycled through four 5 min modes: NO_y, NO_2, NO, and zero (prereactor).

Calibrations were performed twice daily at the tower inlets by standard addition and dynamic dilution of a NO standard (52.1 ppbv, Scott-Marrin, Inc., Riverside, California) and a tower-mounted NO_2 permeation tube maintained at 35°C. The NO_2 permeation rate was determined by conversion to NO on a hot Mo converter with a known efficiency of 99.9 ± 0.5%. This converter was characterized before and after the project by gas-phase titration. The average conversion efficiency of the photolytic converter was found to be 47 ± 11(1σ)%. Artifacts were observed in both the NO and NO_2 signals during the course of the experiment. The NO artifact was determined by averaging the NO signal during the 2 or 3 hours before sunrise and after sunset each day and was found to range from 5 to 60 pptv with a typical value of about 25 pptv. These points were used to calculate a linearly interpolated NO background which was subtracted from each of the 10 s observations in the time series. The uncertainty in the 1-hour-averaged NO mixing ratios is estimated at ±2 pptv (95% confidence level). The NO_2 artifact (17 ± 7(1σ)pptv) was found when passing sample air through the Mo converter followed by the photolytic converter. An increase in signal was observed when the photolysis cell was illuminated. No increase was found when a second Mo converter was installed downstream of the photolytic converter when the cell was not illuminated. This artifact was quantified during the calibrations each day and was subtracted from the NO_2 time series by linear interpolation. Although instrument noise was typically of order of 5-10 pptv, uncertainty in the artifact level increases the detection limit of hour NO_2 averages to about 20 pptv. Since the concentration of NO_y in the "zero air" used during calibrations was not significantly lower than the levels observed in ambient air, the NO_y data was corrected for the NO artifact only.

A tower-mounted mass flow controller reduced the pressure to about 200 torr in the 30 m of black Teflon tubing from the inlets to the analyzer and limited the residence time to about 10 s. A wind-sector signal from a tower-mounted anemometer was used to control a pump which supplied an excess flow of scrubbed air to both inlets during periods when ship exhaust could be aspirated by the instrument. The wind-sector signal was digitally recorded at 30 s intervals and was later used to remove periods of contamination from the CO, ozone, and reactive nitrogen data. Even with this protection, ship exhaust signal spikes interfered with instrument performance and limited the number of reactive nitrogen 10 s data points to 34,953 (NO, 11,894; NO_y, 15,072; NO_2, 7,987) for the period from J.D. 82 to J.D. 112. Although these data only cover approximately 15% of the total time at sea, a considerable portion of the data loss occurred during periods when the ship was stationary. Therefore the data presented here provide an adequate representation of the composition air over the entire region traversed during the voyage.

Measurements of $j(NO_2)$

Measurements of the photolysis rate coefficient of NO_2, $j(NO_2)$, were made using an upward looking 2π steradian (sr) chemical actinometer positioned on top of the 10 m bow tower such that the sky was unobstructed [*Kelley et al.*, 1995]. The actinometer was supplied with the output of a NO_2 permeation tube diluted with ambient air filtered through a charcoal/calcium sulfate scrubber. The resulting mixture showed a NO_2 mixing ratio of 6180 ± 25(1σ) ppbv. Assuming plug flow, the calculated residence time in the exposed section of the tube was about 0.8 s and was corrected for atmospheric temperature and actinometer pressure. A modified commercial chemiluminescence analyzer (Model 42, Thermal Environmental Instruments, Franklin, Massachusetts) measured NO generated by the photolytic dissociation of NO_2 in the actinometer tube. Twice every hour the background concentration of NO in the NO_2/dry air mixture was quantified by switching to a dark path which bypassed the quartz photolysis tube.

Weekly analyzer calibrations were made using a 52.1 ppbv NO standard (Scott-Marrin, Inc., Riverside, California). The detection limit determined during background cycles (30 s, 1:1 S:N, ±2σ) was on the order of 10^{-4} s^{-1}. Since the photolysis rate coefficient is calculated using the ratio of the change in NO concentration to the concentration NO_2,

$$j(NO2) = (\Delta[NO]/[NO2])(1/\Delta t), \qquad (1)$$

the absolute sensitivity of the analyzer to NO is not important to the result. Periodic measurements of the NO_2 permeation tube output were made using a Mo converter at 380°C. Its conversion efficiency was determined to be 99.9 ± 0.5% using gas-phase titration of NO with ozone before and after the cruise. Data reduction and corrections were similar to that described previously [*Kelley et al.*, 1995] with an additional correction for titration of NO by the incidental O_3 in the 35 m return path from the actinometer to the NO detector. The largest corrections were found at the highest photolysis rates and were about 10%. The total uncertainty in the absolute value of $j(NO_2)$ is 9% at the 95% confidence level.

Back Trajectories

Back trajectories were calculated from NOAA's Medium Range Forecast (MRF) database using the Hybrid Single-Particle Langrangian Integrated Trajectories (HY-SPLIT) program [*Draxler et al.*, 1991]. This model was used to calculate analyses for 1000 and 2000 m above the ship's position at 0000 and 1200 UTC for each day of the cruise. Since the marine boundary layer varied from 500 to 2000 m, it should be noted that these calculated trajectories indicate the synoptic situation and general origin of the air mass sampled and should not be interpreted as the literal path traversed by an air parcel.

Results and Discussion

Four distinct air masses, or meteorological regimes, were encountered during the cruise (Figure 1). These have been labeled southern hemisphere maritime extratropical (SHmX), southern hemisphere maritime equatorial (SHmE), northern hemisphere maritime equatorial (NHmE), and northern hemisphere continental tropical (NHcT). The trace gas and aerosol data mirror the changes observed in the meteorology (Figure 2). For purposes of comparison the data have been partitioned into these four groups and are presented in that context (Table 1).

Meteorology and Surface Back Trajectories

Surface winds (on the basis of shipboard observations) in the SHmX regime were the strongest of the cruise (7 m s^{-1} average) with winds starting from the north and backing continuously for the 10 day period. A low centered at about 50°S tracked eastward during the period with a trough extending to near the ship's position at 28°S. Weak high pressure filled in from the west starting J.D. 88. Back trajectories from the period typically show quite long traces across the south Indian and Atlantic Oceans with the air parcels spending much of their time in the zonal flow of the remote marine free troposphere (SHmX in Figure 1). However, toward the end of this period several trajectories pass over South Africa. From 18°S to 22°S the back trajectories show that parcels passed over the nearby island of Madagascar. This 3 day period was probably contaminated by local emissions and therefore is unrepresentative of the large-scale Indian Ocean troposphere.

A large increase in average air and sea surface temperatures was seen in the SHmE while the average wind speed decreased. Winds started from the east but then clocked slowly around to the southwest as an extended trough of low pressure formed to the east of the ship. Most of the back trajectories for this period are influenced by the easterly trade winds and remain entirely over the southern Indian Ocean (SHmE in Figure 2). There was heavy rain for much of the day at 9°S (near the ITCZ), but this was not accompanied by a shift in wind direction or speed.

The ITCZ was entered at about 6°S on J.D. 101. Surface winds, as observed from the ship, were westerly at the ITCZ and slowly backed to the east before becoming light and vari-

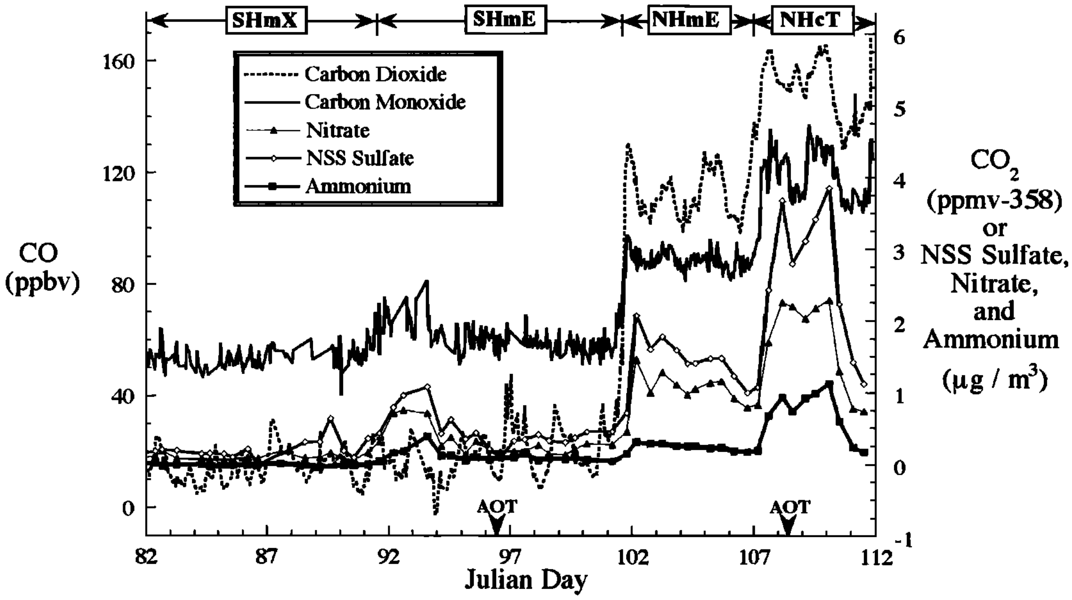

Figure 2. Time series showing strong correlation between CO (ppbv), CO_2 (ppmv - 358 ppmv) and bulk aerosols including ammonium, non-sea-salt (NSS) sulfate and nitrate (µg m^{-3}) for the cruise. CO and CO_2 data have been averaged into 1 hour periods, while aerosol data represents samples typically collected over 12 hour periods. Increased CO and aerosols during Julian Days (J.D.) 91.5-94.3 coincides with close passage to Madagascar, and the islands of Reunion and Maritius. Prior to J.D. 92 the ship was in the SHmX regime and after J.D. 93 the SHmE was entered. The sharp increase at J.D. 101.6 marks the transition across the intertropical convergence zone (ITCZ), while the increase at J.D. 107.0 is the transition from NHmE to NHcT air mass. The AOT markers on the x axis indicate when aerosol optical thickness determinations cited in Table 3 were collected.

Table 1. Surface Observations by Flow Regime

Designation	SHmX	SHmE	NHmE	NHcT
Latitude	34°S to 22°S	18°S to 6°S	6°S to 6°N	4.5°N to 9°N
Julian day	81.0 to 91.5	94.3 to 101 6	101.6 to 107.0	107.0 to 112.0
Meteorological Data				
Average Maximum Air Temperature, °C	25.5 ± 2.4	30.5 ± 1.2	31.5 ± 1.3	31.3 ± 0.8
Average Minimum Air Temperature, °C	21.6 ± 1.6	27.3 ± 0.8	28.7 ± 0.2	28.9 ± 0.4
Sea Surface Temperature, °C	23.7 ± 1.7	29.1 ± 0.6	29.8 ± 0.3	29.9 ± 0.4
Wind Speed, m s^{-1}	6.6 ± 3.0	3.3 ± 9.6	1.9 ± 0.9	3.8 ± 1.5
Trace Gas Data				
[CO], ppbv	54.1 ± 4.0	59.3 ± 3.7	89.0 ± 3.3	120.4 ± 9.8
[O_3], ppbv	17.0 ± 1.8	11.5 ± 2.5	7.5 ± 1.2	15.7 ± 2.9
[CO_2], ppmv	358 ± 0.2	358 ± 0.4	362 ± 0.5	363 ± 1.2
[NO], pptv *	13.6 ± 13	4.8 ± 8.0	4.63 ± 3.15	4.66 ± 4.0
[NO_2], pptv	···	44.3 ± 12	18.9 ± 5.9	38.8 ± 34
[NOy], pptv	165 ± 49	141 ± 34	104 ± 16	178 ± 71
Aerosol Data				
Number of Samples	17	13	12	9
Na^+, μg m^{-3}	2.73 ± 2.17	3.30 ± 0.68	0.47 ± 0.18	1.11 ± 0.44
Cl^-, μg m^{-3}	4.91 ± 4.12	5.83 ± 1.18	0.80 ± 0.33	1.58 ± 0.74
SO_4^{2-}, μg m^{-3}	0.82 ± 0.49	1.19 ± 0.18	1.52 ± 0.34	2.96 ± 1.04
NSS SO_4^{2-}, μg m^{-3}	0.22 ± 0.15	0.36 ± 0.12	1.40 ± 0.36	2.68 ± 0.95
NH_4^+, μg m^{-3}	-0.01 ± 0.02	0.08 ± 0.03	0.24 ± 0.05	0.71 ± 0.33
NO_3^-, μg m^{-3}	0.01 ± 0.04	0.22 ± 0.07	1.01 ± 0.25	1.71 ± 0.62
Mineral dust, μg m^{-3}	< 0.1	< 0.1	< 0.1	6.2 ± 4.4

All average values are shown with ± 1 standard deviation.

SHmX, southern hemisphere marine extratropical; SHmE, southern hemisphere marine equatorial; NHmE, northern hemisphere marine equatorial; NHcT, northern hemisphere continental tropical; ppbv, parts per billion by volume; ppmv, parts per million by volume; pptv, parts per trillion by volume; NSS, non-sea-salt.

* Values for NO are calculated from daytime observations only.

able at the equator. Weak high pressure in the Arabian Sea dominated the flow in this region. Back trajectories starting at 1000 m were quite short and reflect the extremely light easterlies of the region (NHmE in Figure 1). Evidence of the calm winds in this regime is clearly seen in the large decrease in sea-salt aerosol loading (Na^+ and Cl^-, Table 1).

The NHcT regime was ushered in on the morning of J.D. 107 with heavy rain and funnel cloud sighting. Surface winds quickly went from the west to the northeast and remained there for the next three days with surface high pressure over the southern tip of India. Starting with J.D. 108 and continuing for the remainder of the cruise, back trajectories cross southern India and Sri Lanka (NHcT in Figure 1). Closer to the southern tip of India winds veered to the northwest.

Carbon Monoxide, Carbon Dioxide, and Aerosols

Clear indications of the four distinct meteorological regimes can be found in the CO and aerosol time series plotted in Figure 2. The lowest CO and CO_2 levels of the cruise were found in the SHmX regime (54.1 ± 4.0 ppbv and 358 ± 0.2 (1σ) ppmv). This is expected from the remote marine back trajectories and is consistent with recent data from Cape Grim, Australia [*Novelli et al.*, 1994].

Elevated CO is found between J.D. 91 and J.D. 94 (22°S and 18°S). A local maximum in the NO_y and aerosol concentrations is also evident during this period. Emissions from Madagascar are suspected to be the source of these increases, since a number of back trajectories indicate that the ship intercepted air parcels which crossed over the island in the boundary layer. However, the ship also made two close passes (<15 km) to the populated islands of Mauritius and Reunion and are likely to have contributed to the local contamination.

In the SHmE regime the average CO mixing ratio increased by almost 10% to 59.3 ± 3.7 ppbv, even though the source region determined from back trajectories, the remote Indian Ocean, did not change. This rise was accompanied by a significant increase in the concentrations of NSS SO_4^{2-} and NH_4^+. It has been proposed that this is the result of cyclonic flow around local disturbances along the ITCZ which allows SHmE air to cross along the western edge of the disturbances and bring NHmE air down along the eastern edge, causing an increase in CO and aerosols to the south of the ITCZ (Figure 3a) (T. N. Krishnamurti, personal communication, 1995). Traditionally, the most simple model of the ITCZ consists of converging flow from both hemispheres to a continuous area of uniform rising motion that acts as a barrier to cross-hemispheric mixing. More realistically, the ITCZ is an area of discrete cloud clusters separated by regions of relatively clear sky and little convergence. During 3 days in this regime, back trajectories show cross-ITCZ flow (e.g. Figure 3b).

The ITCZ was encountered at 6°S where CO and CO_2 increase sharply and mark the start of the third regime on J.D. 102. Showing a gain of more than 50% over the SHmE regime, the

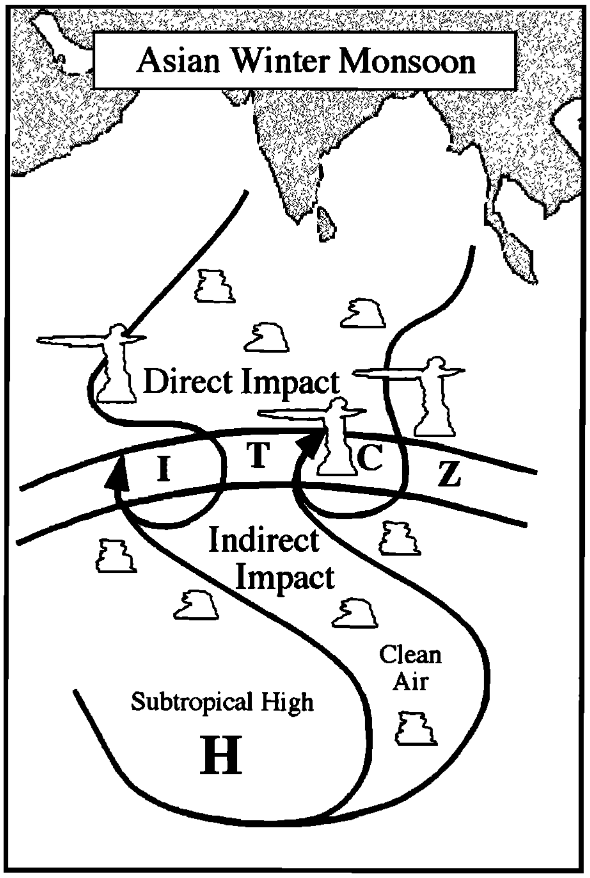

Figure 3a. Counterclockwise circulation around cyclonic disturbances along the ITCZ that has been proposed as a mechanism for interhemispheric mixing within the lower troposphere. It appears as air from the northern hemisphere sweeps around to the east of numerous eddies that are present near the ITCZ and mixes with cleaner air approaching from the south (T. N. Krishnamurti, personal communication, 1995). The consequences of this mixing are visible in the trace gas and aerosol data collected in the SHmE regime.

average CO in the NHmE regime is 89.0 ± 3.3 ppbv, while the CO_2 climbed from 4 ppmv to 362 ppmv. The crossing transition is also clearly observed in the aerosol concentrations. The average levels of NO_3^-, NSS SO_4^{2-}, and NH_4^+ are nearly 4 times higher than in the southern hemisphere. The back trajectories for this period are contained entirely within the northern Indian Ocean and are quite short because of very weak winds.

The transition into the fourth regime occurred during the 3 hours after the passage of a squall line on the morning of J.D. 107. During this period, CO increased from 92 ppbv to 122 ppbv concurrently with dramatic rises in the CO_2 and aerosol concentrations. Filters collected during this episode were dark grey in color and showed significant quantities of mineral dust, suggesting a direct continental impact on the air mass. The back trajectory (1000 m) analyses indicate that the influence of the continent was seen after 2-6 days over the Indian Ocean at a distance of over 1500 km. AVHRR data show high AOT values over the northern regions of the Bay of Bengal; the gradients suggest that the sources lie mostly in India [*Husar et al.*, 1997]. The trajectories obtained in this work suggest that some of the aerosols (and gases) could have been transported across India from this region. In addition, AOT distributions also suggest that there are substantial sources in Bangladesh and northern Burma, possibly caused by biomass burning which peaks during March through May [*Hao and Liu*, 1994].

The relative magnitude of the abrupt changes observed during the transition from the NHmE to the NHcT regime reflect the chemical signature of the emissions from India and can be used to characterize the plume and estimate the degree of photochemical aging. The back trajectories for the NHcT period show 2-6 day transport times at 1000 m altitude, approximately the top of the boundary layer. The lifetimes of CO_2 (~ 15 years) and CO (~ 30 days)[*Khalil and Rasmussen*, 1990] are long compared to the travel times, and we can use ratios of changes in concentrations to account for dilution in the manner of *Crutzen et al.* [1979]. We assume that in India the ratio of anthropogenic emissions of CO, NO_x, and SO_2 to emissions

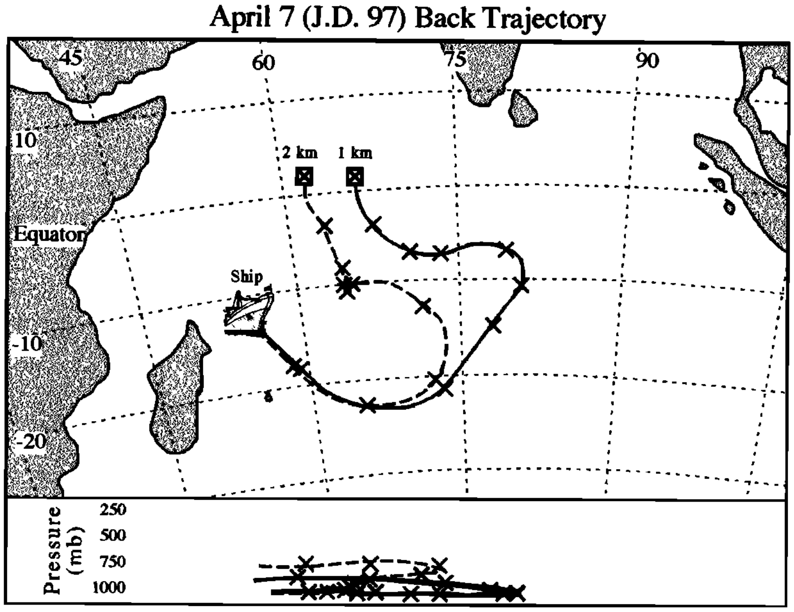

Figure 3b. Ten day back trajectories at 1000 and 2000 m ending at J.D. 97 show an air parcel originating in the northern hemisphere and crossing the ITCZ (6°S). The lower section shows the vertical path of the trajectories as a function of longitude and pressure.

Table 2. Emission Ratios

	Species			
	CO_2	CO	NO_3^- (N)	SO_4^{2-} (S)
U.S. emissions 1994[a]	5150	89	6.5[b]	9.6[c]
U.S. emissions 1960[a]	2900	100	3.9[b]	10[c]
U.S. molar ratios 1994,[d] %		2.7	0.40	0.26
U.S. molar ratios 1960,[d] %		5.4	0.42	0.47
Biomass burning ratios,[d,e] %		10	0.11	0.03
Observed concentration change, ppbv	1700	30	0.43	0.44
U.S. molar ratios 1960,[f] %			7.8	8.7
Plume ratios,[f] %			1.43	1.47
Fraction Remaining,[g] %			18	17

[a] Emissions in teragrams (Tg = 10^{12} g).
[b] Tg nitrogen.
[c] Tg sulfur.
[d] Moles of trace species per mole CO_2.
[e] Biomass ratios from *Crutzen and Andreae* [1990].
[f] Moles of trace species per mole of CO.
[g] Plume ratio divided by U.S. molar ratio 1960

of CO_2 are similar to those of the U.S. prior extensive controls (Table 2). For example, in 1994, U.S. emissions of CO were 2.7% of CO_2, but in 1960 they were 5.4%. In India, wood, dung, and crop residue are important fuels [*Crutzen and Andreae*, 1990], but the NO_x/CO and SO_x/CO emissions ratios are lower than emission ratios from fossil fuel combustion. Biomass burning results in much higher emissions of nitrogen oxides than sulfur oxides; the observed concentrations (Table 2) suggest that such fires did not contribute significantly to the pollutants observed in this study.

The 1960 CO_2 emissions for North America is estimated to be 2900 teragrams (Tg) [Environmental Protection Agency, 1995]. The ratio of moles of CO to moles of CO_2 emitted is calculated as the ratio of the teragrams emitted multiplied by the inverse ratio of the gases' molecular mass which gives 5.4%. Similarly, the molar ratios for the differences between the NHmE air and NHcT air were found. The change in the CO_2 concentration between the two regimes is about 1700 ppbv. The change in CO concentration is about 30 ppbv. Since the concentrations are expressed as volumetric mixing ratios, the ratio of the differences can be found directly giving 1.8%. The observed plume ratio is much less than the emissions ratio (~ 5.4%) and far lower than can be accounted for by OH attack in the short time indicated by the back trajectory analysis. This suggests that noncombustion sources of CO_2 are important. In the dry season, Indian soils emit substantial amounts of CO_2 (*Raich and Potter*, 1995). Our observations are consistent with 3 times as much CO_2 being emitted by soil and plant respiration as by combustion. The abrupt change in CO can primarily be attributed to anthropogenic emissions, and calculation of the ratios for nitrate and sulfate relative to CO provides a framework in which to compare the plume concentrations with the emission inventories. The fraction calculated from the plume ratio divided by the North American emission ratio,

$$\text{fraction remaining} = \frac{(\,\Delta[X]/\Delta[CO]\,)_{\text{Observed}}}{(\,\Delta[X]/\Delta[CO]\,)_{\text{Emission}}} \qquad (2)$$

gives an estimate of material remaining in the plume at the time of sampling. The ratio of changes in nitrate and sulfate to changes in carbon monoxide (Table 2) shows substantial reductions in these reactive species; both nitrate and sulfate are reduced to about 18% of their calculated initial concentrations. This is equivalent to almost two e-folding lifetimes for a travel time of 2-6 days. A lifetime of 1-3 days seems reasonable for conversion of NO_x to nitrate and SO_2 to sulfate and subsequent removal in the absence of precipitation when deposition to the ocean is the main sink.

Surface Ozone

Up to J.D. 107, surface O_3 shows a nearly continuous trend of slowly decreasing concentration with time (Figure 4). Superimposed on this trend is a diurnal cycle of ozone destruction that starts at sunrise, continues until midafternoon, and then is replenished during the night. In the SHmX regime the average O_3 is 17.0 ± 1.8 ppbv and drops to 11.5 ± 2.5 ppbv in SHmE. The lowest levels of O_3 found on the cruise were in the NHmE regime (7.5 ± 1.2 ppbv). In the same 3 hours of J.D. 107 that had large CO increases, hourly averaged ozone also increased from 10.4 ppbv to 15.2 ppbv. In the NHcT region ozone increased to 15.7 ± 2.9 ppbv as continental influence was detected. Figure 5a shows a scatterplot of hourly averaged CO versus O_3 for the whole cruise separated by region. In the first three regimes there is no discernible correlation between ozone and CO. In the continentally impacted area, NHcT, there is positive correlation suggesting a common source of the CO and ozone precursors but the correlation coefficient is statistically insignificant ($r = 0.53$) for a few degrees of freedom.

Significant destruction of ozone was seen in the diurnal cycle for each regime with the lowest midday minima occurring in the two equatorial regions. This cycle is clearly visible in the hour-averaged data (Figure 4), particularly in the equatorial regions. Similar daily oscillations in the ozone mixing ratio were observed by *Johnson et al.* [1990] in the western Indian Ocean during the 1987 SAGA experiment. Near the end of June they observed a diurnal variation of 4 ppbv from 30°S to 10°S, where the ozone mixing ratio was slightly over 20 ppbv. In the present data set, losses of 37% and 30% of the predawn maximum ozone occurred in the SHmE and NHmE regimes, respectively. The lowest levels of O_3 were found in the NHmE regime; ozone peaked at sunrise and reached a minimum just after solar noon. This strong diurnal variation may be caused

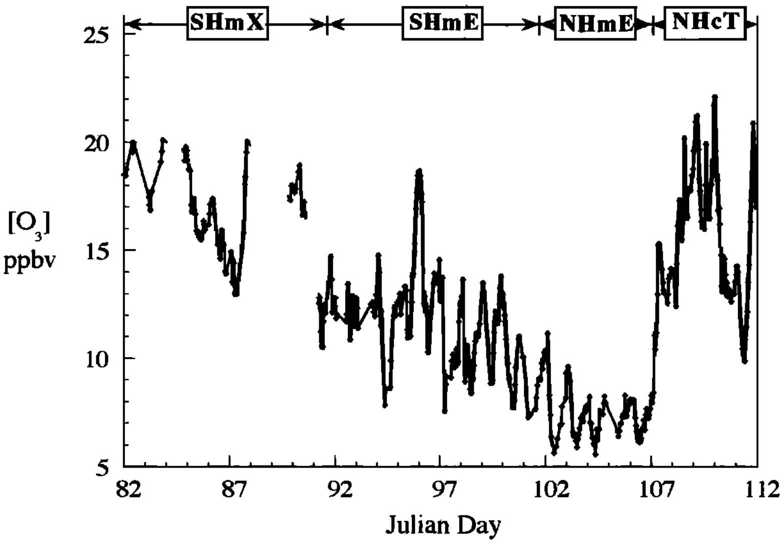

Figure 4. Ozone (parts per billion by volume) time series for the cruise. Data have been averaged into 1 hour periods. Note the strong diurnal variation in the SHmE and NHmE regimes from J.D. 94 to 107 and the rapid rise due to photochemical ozone production entering the NHcT regime on J.D. 107.

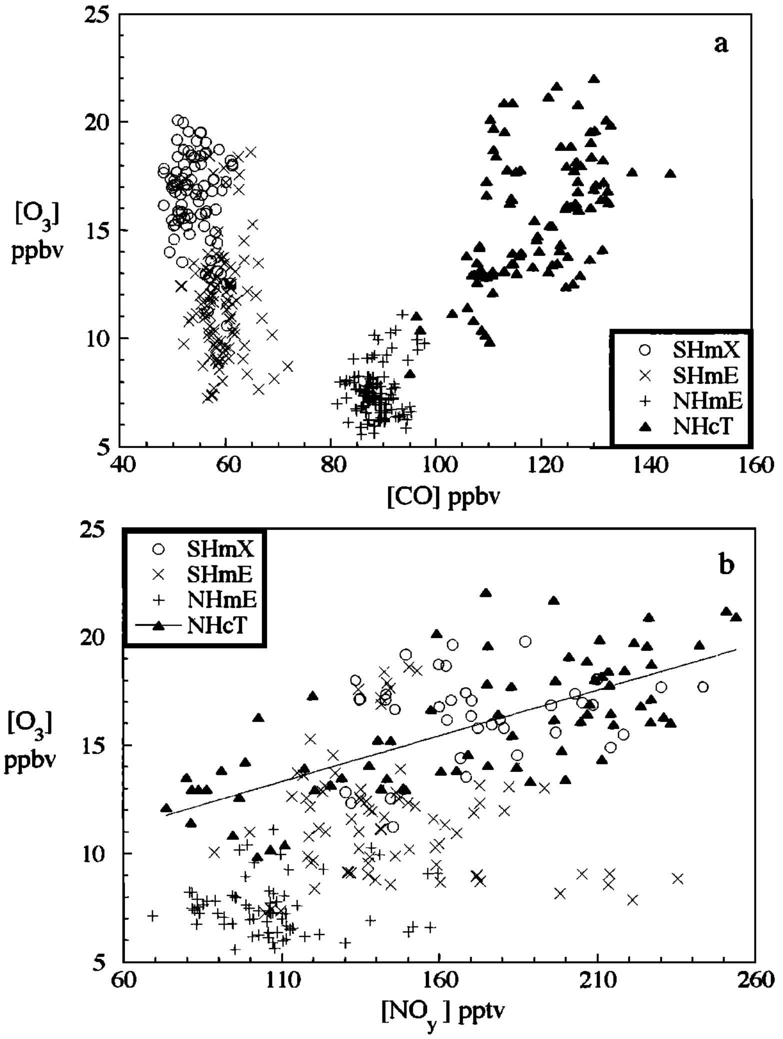

Figure 5. Scatterplots of hour averaged data pairs of (a) CO and O_3 and (b) NO_y and O_3. The contributions from the four meteorological regimes are represented by different symbols. Ozone and NO_y maxima were observed in the most southern and northern regions sampled. In the SHmX regime (open circles), modest levels of ozones were recorded with relatively high NO_y and low CO mixing ratios indicating a region of general subsidence of free tropospheric air. At the northern end of the cruise in the NHcT regime (solid triangles), ozone was positively correlated with NO_y ($r = 0.72$, slope = 0.042), indicating a region of photochemical ozone production.

by reactions involving halogens [e.g.*Vogt et al.,* 1996] and will be presented separately.

NO, NO_2, and NO_y

The gas-phase reactive nitrogen data (Figure 6c), NO_y, show a latitudinal profile similar to surface ozone (Figure 4). The rise in NO_y concentration around J.D. 92 (Figure 6c) is believed to be the result of local emissions from nearby islands. As with surface O_3, the regime maxima of 165 ± 49 and 178 ± 71 pptv occur in the SHmX and NHcT, respectively. Figure 5b displays a scatterplot of hourly averaged NO_y plotted against O_3. Data from the SHmX ($r = 0.21$, slope = 0.014) and NHcT ($r = 0.72$, slope = 0.042) regions show a positive correlation; however, only the correlation in the NHcT regime is significant. This relationship is consistent with measurements obtained during the four Mauna Loa Observatory Photochemistry (MLOPEX) 2 intensives and MLOPEX 1. During these experiments the relationship between O_3 and NO_y was characterized by correlation coefficients in the range of 0.7-0.8 and slopes ranging from 0.06-0.14 ppbv/pptv [*Brasseur et al.,* 1996]. The average observed NO_y/O_3 ratios for each regime range from about 10 to 14 (pptv/ppbv). These values are on the upper end of ratios observed during the MLOPEX projects. *Murphy et al.* [1993] found that this ratio ranged from 5 to 25 (pptv/ppbv) in the tropical upper troposphere near Darwin, Australia. Viewed in the context of the low aerosol loading and the low concentrations of CO, the coincident high levels of NO_y and ozone in the SHmX region suggest that downward transport from the upper troposphere or stratosphere may be the primary source of the air mass. The climatology of the region supports this conclusion, since this period is the rainy season in the south-

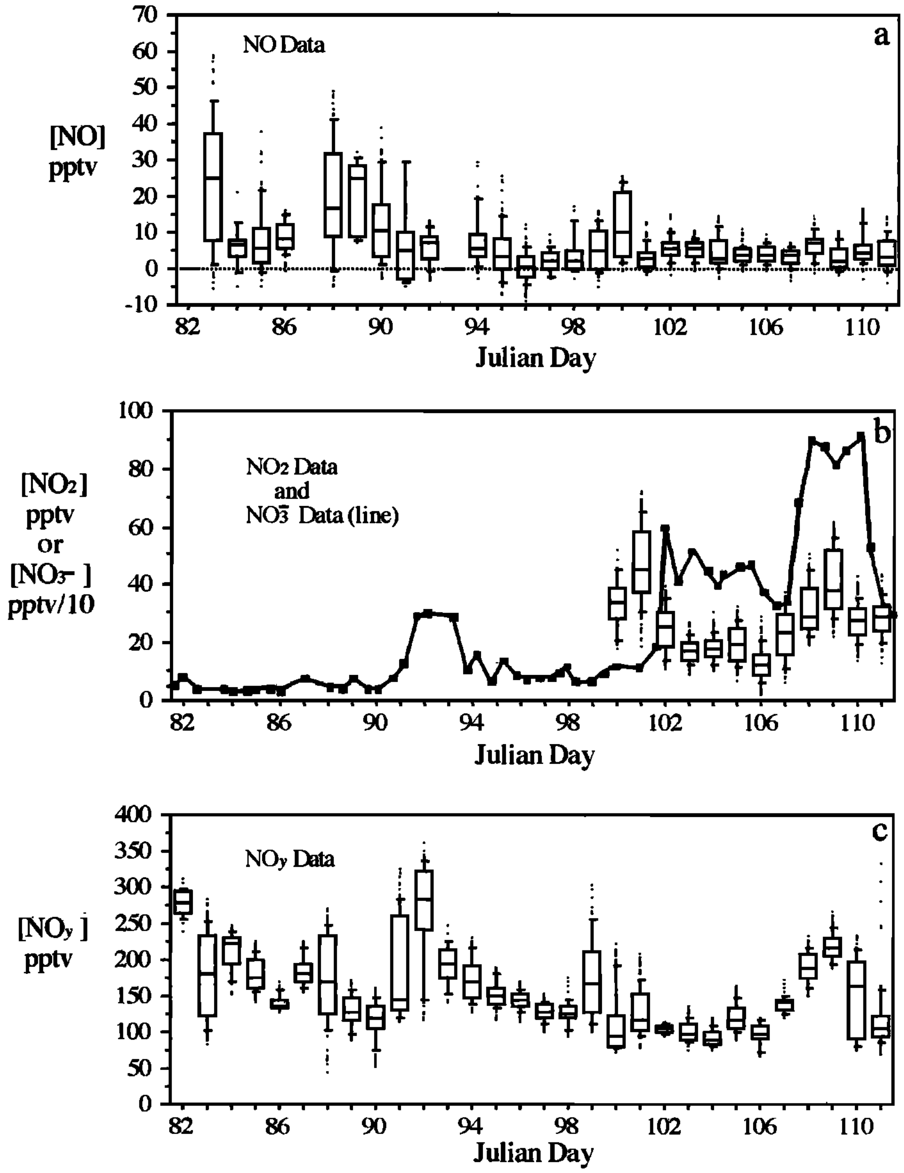

Figure 6. (a) NO, (b) NO_2, and (c) NO_y minute-averaged mixing ratio distributions for each day of the cruise. The box plots within each figure show data distribution; bottom (25%), middle (50%), and top (75%) horizontal box lines indicate the quartiles. The horizontal lines at the bottom and top of the vertical whiskers emanating from each box indicate the 10% and 90% percentiles. Data points beyond the 10% and 90% percentiles are displayed as dots. Aerosol nitrate data (equivalent pptv/10) are shown in Figure 6b for comparison.

ern hemisphere and lightning associated with deep convective activity is common. In contrast, the increase in the NO_y mixing ratio in the NHcT regime was accompanied by increased levels of ozone, CO and aerosols. Thus the NO_y increase in this region can be attributed to emissions from India followed by photochemistry in the air mass during passage over the Indian Ocean.

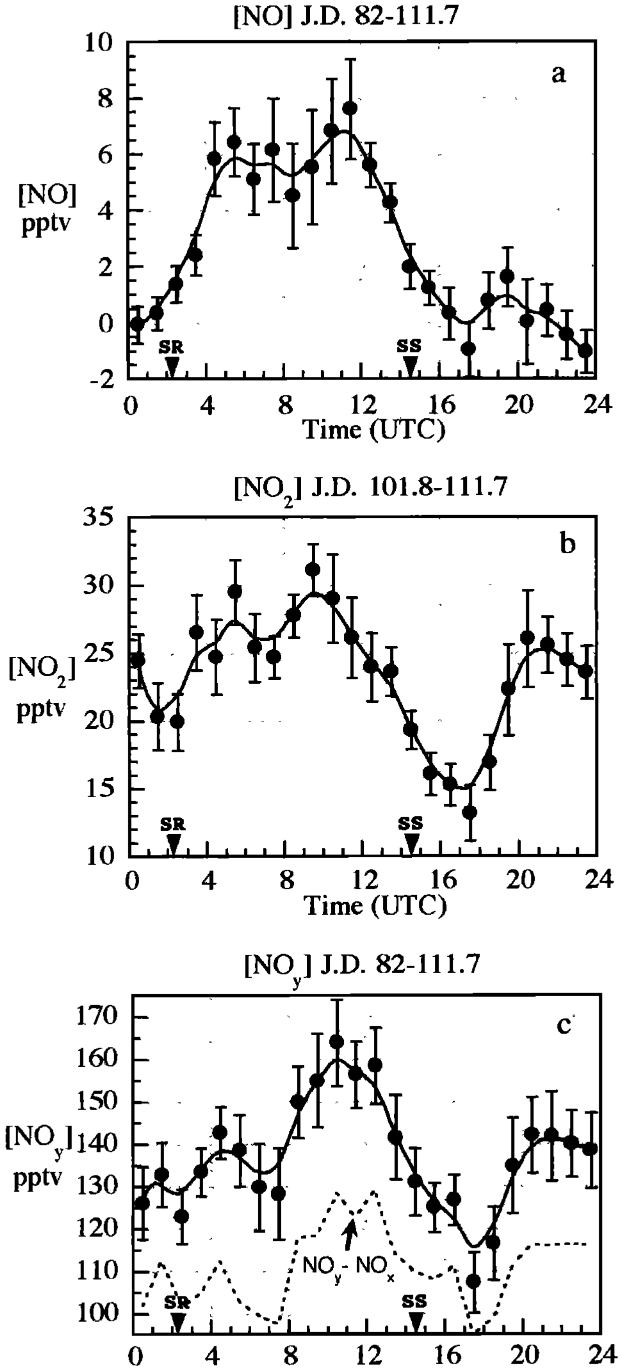

Figure 7. (a) NO, (b) NO_2, and (c) NO_y average diurnal variations calculated from the median values of minute data for each hour. Adjustments were made to observation times so that for each day sunrise, solar noon, and sunset would occur at 0230, 0930, and 1430 UTC, respectively (indicated on plots as SR, sunrise and SS, sunset). Error bars shown indicate 95% confidence intervals.

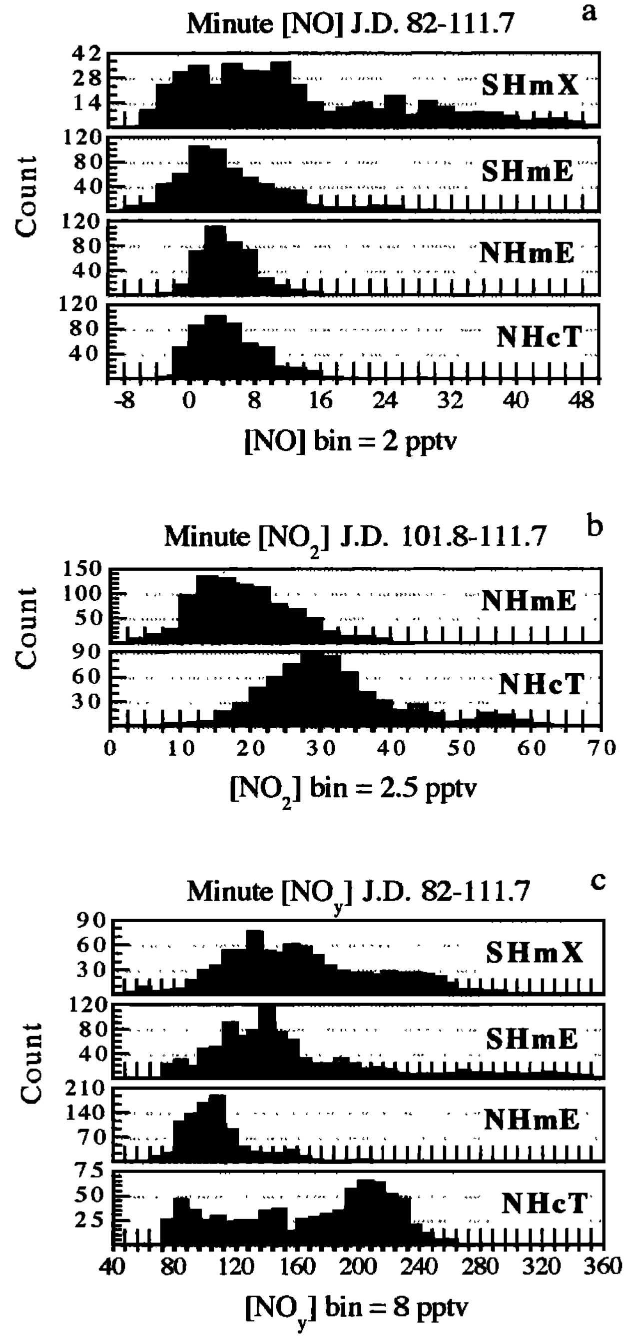

Figure 8. (a) NO, (b) NO_2, and (c) NO_y minute averaged data displayed as histograms. Bars for each mixing ratio interval indicate the total number of observations and are divided to show the contribution from each region.

The daytime NO mixing ratios shown in Figure 6a do not show clear distinctions among the four regimes. The mean values for each regime shown in Table 1 were calculated by averaging observations made each day between sunrise and sunset. From the total of 11,894 ten second NO measurements, 6919 daytime values were used to calculate 1952 one minute averages which were combined to generate statistics for each day and region. Taken as a single population, the minute averages give a NO concentration of 6.78 ± 0.4 ppt (95% confidence level in the mean) for the Indian Ocean. The highest NO concentrations were encountered on J.D. 83 shortly after departure from Durban. As the ship moved away from the continent to the southeast, the NO levels fell off sharply. Back trajectories for this period (J.D. 84-86) show that the air encountered passed to the south of Africa and originated from the remote southern Atlantic Ocean. On J.D. 86 the ship turned to the northeast and the impact of the continental outflow on the NO concentrations can once again be seen in the data over the course of the following few days. This period coincides with the transition from winds originating in the southern Atlantic to flow from the eastern Indian Ocean. By J.D. 95, the midday NO mixing ratio decreased to 5 pptv and little variation in the daily averages was observed during the remainder of the trip except for a slight increase observed around the ITCZ.

The diurnal variations in the median reactive nitrogen mixing ratios are shown in Figure 7. The medians for each hour were determined by separating the minute data for each gas into 24 one hour bins. Before binning, the time stamp associated with each average was normalized to a longitude of 55°E such that daylight hours are synchronous. At this latitude, sunrise occurred at about 0230 UTC and sunset at 1430 UTC. The magnitude of the diurnal variation of NO is similar to observations made in the remote Pacific [e.g., *McFarland et al.*, 1979; *Torres and Thompson*, 1993] and in the North Atlantic for marine air masses [*Dickerson et al.*, 1995]. The daily cycle of NO_y with the sum of NO and NO_2 (NO_x) subtracted (Figure 7c) shows an increase in the late morning hours with a maximum in the afternoon followed by a decline that reaches a minimum about an hour after sunset. The rise in the morning may be explained by the increase in the conversion of NO_x to other components of NO_y with increasing solar radiance and the growth of the boundary layer promoting the downward mixing of photochemically processed air from aloft. In the afternoon, surface deposition dominates production, leading to the observed decrease in NO_y.

Histograms of the nitrogen data shown in Figure 8 illustrate the distribution of the minute averages in the four regimes. Each bar shows the total number of values within the concentration range of the bin and is broken down by regime. The wide distributions of the NO and NO_y data for the SHmX regime confirm the assertion that this region was dominated by a mixture of air masses with vastly different histories. The NO_2 plot (Figure 8b) clearly shows two distinct populations associated with the NHmE and NHcT regimes. As a crude check of the consistency between the NO_x, ozone and NO_2 photolysis rate measurements , the steady state concentration of NO_2 was calculated for each regime using an equation derived from the three step Leighton photostationary state mechanism [*Leighton*, 1961]. The observed NO_2 values exceed the calculated concentrations by about 30 pptv confirming the uncertainty estimate of ±20 pptv in the NO_2 observations (as noted in the Experimental Techniques section).

NO_2 Photolysis Rate and Aerosol Optical Depth

There was a significant reduction in the measured peak NO_2 photolysis rate in the NHcT region relative to the other regimes. Figure 9 shows the photolysis rates on J.D. 96 (SHmE) and J.D. 108 (NHcT), two of the most cloud-free days during the cruise. During the 2 hours surrounding solar noon the average $j(NO_2)$ for J.D. 96 was 8.4 x 10^{-3} s^{-1}, while for J.D. 108 it was 7.5 x 10^{-3} s^{-1}, a difference of 11%. As noted in the hourly deck log, cloud cover was only one eighth to one quarter of the sky during both periods. The Sun was more nearly overhead on J.D. 108 (minimum solar zenith angle of 2.0°) than on J.D. 96 (minimum zenith angle of 19.4°). Table 3 shows the results of the aerosol optical thickness (AOT) measurements and aerosol loadings that were collected during the morning hours of these 2 days. The AOT values observed on J.D. 96 of ~ 0.1 (500 nm) compare well with background values determined in California under clear sky conditions [*Kaufman et al.*, 1994]. The AOT measurements collected on J.D. 108 are systematically higher as a result of the increased aerosol loading in the outflow from India. The filters removed from the aerosol collector on the morning and evening of J.D. 108 were visibly blackened. Results from observations and calculations of AOT and $j(NO_2)$ in Maryland suggest that such a reduction at low zenith angles is the result of a greater degree of absorption (lower single-scattering albedo) in the aerosol collected in the plume from India

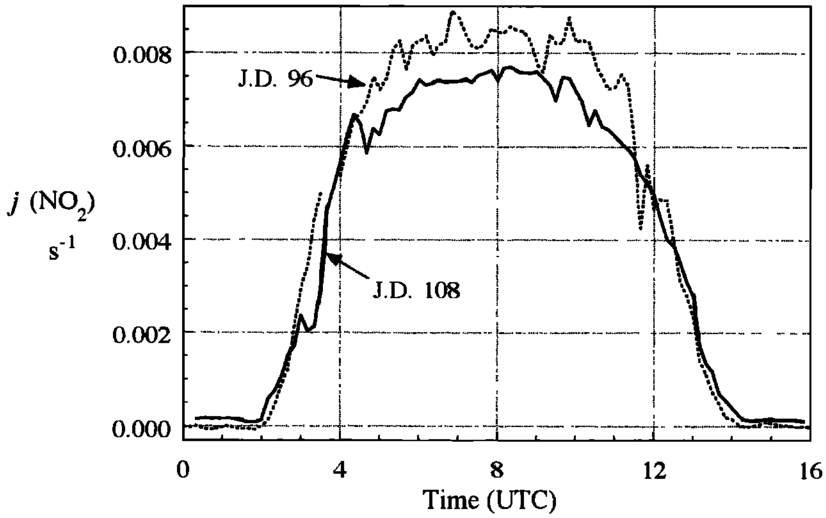

Figure 9. Comparison of NO_2 photolysis rates for J.D. 96 and 108 measured with an upward looking chemical actinometer. The observed aerosol optical depth at 500 nm was 0.13 on J.D. 96 and 0.26 on J.D. 108. The 11% reduction in NO_2 photolysis and the two fold increase in optical depth are believed to be the result of increased loading of aerosol with a high imaginary index of refraction in the outflow from India.

Table 3. Aerosol optical thickness (AOT) measurements

	J.D. 96	J.D. 108	(J.D. 108 - J.D. 96)
AOT			
at 500, nm	0.129 ± 0.001	0.262 ± 0.011	0.133
at 675, nm	0.099 ± 0.004	0.173 ± 0.003	0.074
at 875, nm	0.065 ± 0.003	0.100 ± 0.004	0.035
at 945, nm	0.654 ± 0.007	0.993 ± 0.029	0.339
NSS aerosols			
NSS SO_4^{-2}, μg m^{-3}	0.096	2.80	2.70
NH_4^+, μg m^{-3}	0.01	0.74	0.73
Mineral dust, μg m^{-3}	< 0.01	9.28	9.28
Total, μg m^{-3}	0.1	12.82	12.7

J.D., Julian day; NSS, non-sea-salt.

than is commonly present in aerosol of the eastern United States [*Kondragunta et al.*, 1996].

An important question in accessing the scope of the climate impact of such emissions is whether the aerosol plume was confined to the boundary layer or was carried by zonal flow with the potential of influencing the radiative properties of the entire region? A crude estimate of the thickness of a uniformly polluted layer can be made using the difference in the optical depths (0.13 at 500 nm) and the change in the aerosol loadings. Assuming that the extinction was due totally to non-sea-salt particles, the difference in the total (ammonium, sulfate, and mineral) aerosol loading (L) for the two time periods is 12.7 μg m^{-3}. Using a generic aerosol mass scattering efficiency (S) of 3 m^2 g^{-1} [*Waggoner et al.*, 1981], the thickness of the layer (D) can be estimated as,

$$D = (\mathrm{AOT}) / (S \times L), \qquad (3)$$

which gives a layer of about 4.7 km in depth. Despite the simplistic nature of the estimate, the result suggests that the polluted airmass extended well above the marine boundary layer which was typically observed at about 1-2 km in the sonde data.

Conclusions

A number of atmospheric trace species were measured over the Indian Ocean in order to assess the potential for anthropogenic emissions to modify tropospheric chemistry across the ITCZ. Major findings are as follows.

1. In transecting the Indian Ocean from Durban, South Africa, to Colombo, Sri Lanka, four distinct meteorological regimes were found in the spring of 1995. Average CO increased with latitude going from 33°S to 9°N and was closely mirrored by increases in aerosol loading. Across the ITCZ at 6°S the NSS SO_4^{2-} concentration increased by a factor of 4. The strong latitudinal gradient in aerosol concentrations measured on this cruise is consistent with the areal distribution of aerosol optical thickness (AOT) as measured by AVHRR [*Husar et al.*, 1997] in the spring. AVHRR shows a strong gradient in AOT with highest values over the Arabian Sea, decreasing sharply in the region 10°N to the equator; this is the region where the ship experienced a shift in air mass trajectories from NHmE to NHcT (Figure 1) and a sharp increase in the concentration of aerosols and CO.

2. Despite the increased CO and aerosol concentrations found in the SHmE regime, back trajectories indicate that both it and the SHmX regime share the remote Indian Ocean as the immediate source region. As the ITCZ was approached, back trajectories show northern hemisphere air circulating to the east of localized disturbances along the ITCZ and mixing with southern hemisphere air. This cross-ITCZ flow is believed to be the cause of the increased levels of pollutants measured in this region.

3. Strong evidence of direct transport of anthropogenic emissions was seen 1500 km from southern India. Sharp increases in CO, CO_2, O_3, NO_y, NSS sulfate, ammonium, and nitrate aerosols were detected. A comparison of the pollutant levels observed in the plume from India with North American emission inventories suggests that the air masses sampled were substantially depleted in soluble species.

4. Total gaseous reactive nitrogen paralleled surface ozone in its latitudinal profile with maxima in the most southern and northern regions sampled. In the southern hemisphere the correlation with ozone may be attributable to downward transport from the stratosphere or lightning, while the increase observed near the coast of India can be accounted for by conventional photochemistry. A strong diurnal variation in ozone was observed in the equatorial regions of both hemispheres. The low levels of NO encountered indicate that most of marine boundary layer over the Indian Ocean is an region of active photochemical ozone destruction.

5. The nitrogen dioxide photolysis rate coefficient measured with an upward looking chemical actinometer showed an 11% reduction in an air mass encountered downwind of India when compared to values obtained farther south during the cruise. The aerosol loadings in the region near India were 4 times greater than in the more southern regime. A comparison of the optical depth measurements for these regions showed an increase of 0.13, suggesting that the aerosol had a substantial absorptive element such as mineral dust or soot.

Acknowledgments. Thanks go to the captain and crew of the R/V *Malcolm Baldrige* ; they provided transportation, food, equipment, help, and humor for 33 long days. We are grateful to R. Pinker and F. Miskolczi for providing their assistance in the optical depth measurements. We thank Rik Wanninkhof and Dave Ho of AOML for providing the CO_2 data that they collected during the voyage. We extend thanks to T. Krishnamurti for providing insight into the unique meteorology of the Indian Ocean. We also extend our appreciation to P. J. Crutzen for his insightful comments during the preparation of this manuscript. This work was funded primarily by the Center for Clouds, Chemistry and Climate, which is sponsored by the National Science Foundation and through grants NSF ATM9204047 and ATM9414846.

References

Ackerman, S. A., and S. K. Cox, Surface weather observations of atmospheric dust over the southeast summer monsoon region, *Meteorol. Atmos. Phys.*, *41*, 319-349, 1989.

Andreae, M. O., et al., Biomass burning in the global environment: First results from the IGAC-BIBEX field campaign STARE/TRACE-A/SAFARI-92, in *Global Atmospheric-Biospheric Chemistry*, edited by R. G. Prinn, pp. 83-101, Plenum, New York, 1994.

Baldy, S., G. Ancellet, M. Bessafi, A. Badr, and D. Lan Sun Luk, Field observations of the vertical distribution of tropospheric ozone at the island of Reunion (southern tropics), *J. Geophys. Res.*, *101*, 23835-23849, 1996.

Brasseur, G. P., D. A. Hauglustaine, and S. Walters, Chemical compounds in the remote Pacific troposphere: Comparison between MLOPEX measurements and chemical transport model calculations, *J. Geophys. Res.*, *101*, 14795-14813, 1996.

Cadet, D., Meteorology of the Indian summer monsoon, *Nature*, *279*, 261-267, 1979.

Carroll, M. A., et al., Measurements of nitric oxide and nitrogen dioxide during the Mauna Loa Observatory Photochemistry Experiment, *J. Geophys. Res.*, *97*, 10361-10374, 1992.

Carsey, T. P., D. D. Churchill, M. L. Farmer, C. J. Fischer, A. A. Pszenny, V. B. Ross, E. S. Saltzman, M. Springer-Young, and B. Bonsang, Nitrogen oxides and ozone production in the North Atlantic marine boundary layer, *J. Geophys. Res.*, *102*, 10653-10665, 1997.

Chester, T., A. S. Berry, and K. J. T. Murphy, The distributions of particulate atmospheric trace metals and mineral aerosols over the Indian Ocean, *Marine Chemistry*, *34*, 261-290, 1991.

Crutzen, P. J. and M. O. Andreae, Biomass burning in the tropics: Impact on atmospheric chemistry and biogeochemical cycles, *Science*, *250*, 1669-1678, 1990.

Crutzen, P. J., L. E. Heidt, J. P. Kranec, W. H. Pollock, W. Seiler, Biomass burning as a source of atmospheric gases CO, H_2, N_2O, NO, CH_3Cl, and COS, *Nature*, *282*, 253-256, 1979.

Dickerson, R. R., and A. C. Delany, Modifications of a commercial gas filter correlation CO detector for enhanced sensitivity, *J. Atmos. Oceanic Technol.*, *5*, 424-431, 1988.

Dickerson, R. R., B. G. Doddridge, and K. P. Rhoads, Large-scale pollution of the atmosphere over the remote North Atlantic Ocean: Evidence from Bermuda, *J. Geophys. Res.*, *100*, 8945-8952, 1995.

Doddridge, B. G., R. R. Dickerson, T. G. Spain, S. J. Otmans, and P. C. Novelli, Carbon monoxide measurements at Mace Head, Ireland, in *Proceedings of the Quadrennial Ozone Symposium 1992*, edited by R. D. Hudson, pp. 134-137, NASA, Greenbelt, Md. 1994.

Draxler, R., R. Dietz, R. J. Lagomarsino, and G. Start, Across North America Tracer Experiment (ANATEX): Sampling and analysis, *Atmos. Environ.*, *25*, 2815-2836, 1991.

Environmental Protection Agency, National air pollutant emission trends 1990-1994, Rep. EPA-454/R-95-011, Washington, D. C.,Oct., 1995.

Fehsenfeld F. C., et al., A ground-based intercomparison of NO, NO_x, and NO_y measurement techniques, *J. Geophys. Res.*, *92*, 14710-14722, 1987.

Galloway, J. N., and A. Gaudry, The composition of precipitation on Amsterdam Island, Indian Ocean, *Atmos. Environ.*, *18*, 2649-2656, 1984.

Hao, W. M., and M.H. Liu, Spatial and temporal distribution of tropical biomass burning, *Global Biogeochemical Cycles*, *8*, 495-503, 1994.

Husar, R. B., J. M. Prospero, and L. L. Stowe, Characterization of tropospheric aerosols over the oceans with the NOAA/ AVHRR optical thickness product, *J. Geophys. Res.*, in press, 1997.

Johnson, J. E., R. H. Gammon, J. Larsen, T. S. Bates, S. J. Oltmans, and J. C. Farmer, Ozone in the marine boundry layer over the Pacific and Indian Oceans: Latitudinal gradients and diurnal cycles, *J. Geophys. Res.*, *95*, 11847-11586, 1990.

Kaufman, Y. J., A. Gitelson, A. Karnieli, E. Ganor, R. S. Fraser, T. Nakajima, S. Mattoo, B. N. Holben, Size distribution and scattering phase function of aerosol particles retrieved from sky brightness measurements, *J. Geophys. Res.*, *99*, 10341-10356, 1994.

Kelley, P., R. R. Dickerson, W. T. Luke, and G. L. Kok, Rate of NO_2 photolysis from the surface to 7.6 km altitude in clear-sky and clouds, *Geophys. Res. Let.*, *22*, 2621-2624, 1995.

Khalil, M. A. K., and R. A. Rasmussen, The global cycle of carbon monoxide: Trends and mass balance, *Chemosphere*, *20*, 227-242, 1990.

Kley, D., and M. McFarland, Chemiluminescence Detector for NO and NO_2, *Atmos. Tech.*, *12*, 63-69, 1980.

Kondragunta, S., R. R. Dickerson, G. Stenchikov, P. Kelley, W. F. Ryan, and B. Holben, The Effect of Urban Aerosols on the Rate of Photochemical Smog Formation, *Eos Trans. AGU*, *77(17)*, Spring Meet. Suppl., S64, 1996.

Leighton, P. A., *Photochemistry of Air Pollution*, 300 pp., Academic, San Diego, Calif., 1961.

Luke, W. T., and R. R. Dickerson, The flux of reactive nitrogen compounds from eastern North America to the western Atlantic Ocean, *Global Biogeochem. Cycles*, *1*, 329-343, 1987.

Malingreau, J. P., G. Stephens, and L. Fellows, Remote sensing of forest fires: Kalimantan and North Borneo in 1982-83, *Ambio*, *14*, 314, 1985.

McFarland, M., D. Kley, J. W. Drummond, A. L. Schmeltekopf, and R. H. Winkler, Nitric oxide measurements in the equatorial Pacific region, *Geophys. Res. Lett.*, *6*, 605-608, 1979.

Moody, J. L., A. P. Pszeny, A. Gaundry, W. C. Keene, J. N. Galloway, and G. Polian, Precipitation composition and its variability in the southern Indian Ocean: Amsterdam Island, 1980-1987, *J. Geophys. Res.*, *96*, 20769-20786, 1991.

Murphy, D. M., D. W. Fahey, M. H. Proffitt, S. C. Liu, K. R. Chan, C. S. Eubank, S. R. Kawa, and K. K. Kelly, Reactive nitrogen and its correlation with ozone in the lower stratosphere and upper troposphere, *J. Geophys. Res.*, *98*, 8751-8773, 1993.

Novelli, P. C., K. A. Masarie, P. P. Tans, and P. M. Lang, Recent changes in atmospheric carbon monoxide, *Science*, *263*, 1587-1589, 1994.

Nunnermacker, L. J., Calibration and detection techniques for trace nitrogen compounds in the atmosphere, Ph.D. dissertation, Dep. of Chem., Univ. of Maryland, College Park, 1990.

Pinker, R. T., G. Idemudia, and T. O. Aro, Characteristic aerosol optical depths during the Harmattan season in sub-Saharan Africa, *Geophys. Res. Lett.*, *21*, 685-688, 1994.

Piotrowicz, S. R., C. J. Fischer, and R. S. Artz, Ozone and carbon monoxide over the North Atlantic during a boreal summer, *Global Biogeochem. Cycles*, *4*, 215-224, 1990.

Poulida, O. , K. L. Civerolo, and R. R. Dickerson, Observations and tropospheric photochemistry in central North Carolina, *J. Geophys. Res.*, *99*, 10553-10563, 1994.

Prodi, F., G. Santachiara, and F. Olioski, Characterization of aerosols in marine environments (Mediterranean, Red Sea, and Indian Ocean), *J. Geophys. Res.*, *88*, 10957-10968, 1983.

Prospero, J. M., Aeolian transport to the World Ocean, in *The Sea*, vol. 7, *The Oceanic Lithosphere*, edited by C. Emiliani, pp. 801-974, Wiley-Interscience, New York, 1981.

Prospero, J. M., and D. L. Savoie, Effect of continental sources on nitrate over the Pacific Ocean, *Nature*, 339, 687-689, 1989.

Raich, J. W. and C. S. Potter, Global patterns of carbon dioxide emissions from soils, *Global Biogeochem. Cycles* , *9*, 23-36, 1995.

Ridley, B. A., M. A. Carroll, A. L. Torres, E. P. Condon, G. W. Sachse, G. F. Hill, and G. L. Gregory, An intercomparison of results from ferrous sulphate and photolytic converter Techniques for measurements of NO_x made during the NASA GTE/CITE 1 aircraft program, *J. Geophys. Res.*, *93*, 15803-15811, 1988.

Savoie, D. L., and J. M. Prospero, Particle size distributions of nitrate and sulfate in the marine atmosphere, *Geophys. Res. Lett.*, *9*, 1207-1216, 1982.

Savoie, D. L., J. M. Prospero, and R. T. Nees, Nitrate, non-sea-salt sulfate and mineral aerosol over the North Western Indian Ocean, *J. Geophys. Res.*, *92*, 933-942, 1987.

Savoie, D. L., J. M. Prospero, and E. S. Saltzman, Non-sea-salt sulfate, and nitrate in tradewind aerosols at Barbados: Evidence for long-range transport, *J. Geophys. Res.*, *94*, 5069-5080, 1989a.

Savoie, D. L., J. M. Prospero, J. T. Merrill and M. Uematsu, Nitrate in the atmospheric boundary layer of the tropical South Pacific: Implications regarding sources and transport, *J. Atmos. Chem.*, *8*, 391-415, 1989b.

Savoie, D. L., J. M. Prospero, S. J. Oltmans, W. C. Grausten, K. K. Turekian, J. T. Merrill, and H. Levy, Sources of nitrate and ozone in the marine boundary layer of the tropical North Atlantic, *J. Geophys. Res.*, *97*, 11575-11589, 1992.

Torres, A. L., and A. M. Thompson, Nitric oxide in the equatorial Pacific boundary layer: SAGA 3 measurements, *J. Geophys. Res.*, *98*, 16949-16954, 1993.

Vogt, R., P. J. Crutzen, and R. Sander, A new mechanism for bromine and chlorine release from sea-salt aerosol in the unpolluted marine boundry layer, *Nature*, *382*, 327-330, 1996.

Waggoner, A. P., R. E. Weiss, N. C. Ahlquist, D. S. Covert, S. Will, and R. J. Charlson, Optical characteristics of atmospheric aerosols, *Atmos. Environ.*, *15*, 1891-1909, 1981.

Wanninkhof, R., and K. Thoning, Measurement of fugacity of CO2 in surface water using continuous and discrete sampling methods, *Mar. Chem.*, *44*, 189-205, 1993.

T. P. Carsey and M. Farmer, Atlantic Oceanographic and Meteorological Laboratory, NOAA, Miami, FL 33149.

R. R. Dickerson and P. Kelley, Department of Meteorology, University of Maryland, College Park, MD 20742. (e-mail: russ@atmos.umd.edu; paulk@atmos.umd.edu)

J. M. Prospero and D. L. Savoie, Rosenstiel School of Marine and Atmospheric Science, University of Miami, Miami, FL 33149.

K. P. Rhoads, Department of Chemistry, University of Maryland, College Park, MD 20742. (e-mail: rhoads@atmos.umd.edu)

(Received November 13, 1996; revised April 4, 1997;
accepted April 9, 1997.)